

The contrast between monovalent and multivalent metal battery anodes

Yuanjian Li^{1†}, Sonal Kumar^{1†}, Gaoliang Yang^{1†}, Jun Lu^{2*}, Yan Yao^{3*}, Kisuk Kang^{4*}, Zhi Wei Seh^{1*}

¹Institute of Materials Research and Engineering (IMRE), Agency for Science, Technology and Research (A*STAR), 2 Fusionopolis Way, Innovis #08-03, Singapore 138634, Republic of Singapore

²College of Chemical and Biological Engineering, Zhejiang University, Hangzhou, 310027, People's Republic of China

³Department of Electrical and Computer Engineering and Texas Center for Superconductivity at the University of Houston (TcSUH), University of Houston, Houston, Texas 77204, United States

⁴Department of Materials Science and Engineering, Institute for Rechargeable Battery Innovations, Research Institute of Advanced Materials, Seoul National University, Seoul 08826, Republic of Korea

[†]These authors contributed equally to this work

* Email: junzoelu@zju.edu.cn, yyao4@uh.edu, matlgen1@snu.ac.kr and sehzw@imre.a-star.edu.sg

Abstract: Monovalent (lithium, sodium, potassium) and multivalent (magnesium, calcium, aluminum) metal anodes are promising alternatives to graphite anodes for overcoming the performance limitations of lithium-ion batteries. In this review, we compare and contrast their electrochemical behaviors in nonaqueous electrolytes by discussing their common challenges ~~of, including~~ irregular metal deposition and unstable solid electrolyte interphases (SEIs), as well as their unique differences due to dissimilar surface energies and cation charge densities. General design strategies for electrode, electrolyte, and interphase are proposed to enable horizontally deposited metals with preferred crystallographic orientations, and stable SEIs with distinct chemical compositions yet similar structural homogeneity. Finally, we assess the specific advantages and unresolved challenges of each system, providing cross-disciplinary insights to advance high-energy and low-cost metal anode batteries for next-generation energy storage.

Since their commercialization in 1991, lithium (Li)-ion batteries (LIBs) have revolutionized the fields of communication and transportation, leading modern society into a wireless and sustainable future (1, 2). However, after over 30 years of research and development, state-of-the-art LIBs using conventional graphite anodes (with a theoretical specific capacity of $\sim 372 \text{ mAh g}^{-1}$) are approaching their energy density ceiling of $\sim 300 \text{ Wh kg}^{-1}$ (3, 4). To meet the ever-increasing demands for long-range electric vehicles (EVs) and large-scale energy storage, Li-metal batteries (LMBs) are reviving due to the large theoretical specific capacity (3860 mAh g^{-1}) and negative redox potential (-3.04 V versus standard hydrogen electrode) of Li metal anode (5, 6). The integration of Li metal anodes and lithium-rich transition metal oxide (Li-TMO) cathodes has recently enabled ampere-hour (Ah) scale pouch-type LMBs with a cell-level energy density of $\sim 710 \text{ Wh kg}^{-1}$ (7). Transition to Li-S and Li-O₂ batteries further boosts the energy density to over 750 Wh kg^{-1} (8) and 860 Wh kg^{-1} (9), respectively, which can potentially enable EV ranges exceeding 500 km.

At the same time, concerns over the limited reserves ($< 0.002 \text{ wt}\%$ in the earth's crust) of Li resources have driven extensive efforts toward developing alternative batteries based on earth-abundant ($> 2.0 \text{ wt}\%$) metal anodes, including sodium (Na), potassium (K), magnesium (Mg), calcium (Ca), and aluminum (Al) (10-12). Similar to Li, these post-Li metals are prime anode candidates for high-energy-density batteries because they can offer the highest theoretical specific capacities for each battery type and permit the use of high-energy metal-free cathode materials, such as chalcogens, halogens, and gases (13, 14). Among monovalent and multivalent metals, Mg (3833 mAh cm^{-3}), Ca (2073 mAh cm^{-3}), and Al (8046 mAh cm^{-3}) possess higher theoretical volumetric capacities than Li (2062 mAh cm^{-3}), Na (1128 mAh cm^{-3}) and K (591 mAh cm^{-3}) due to multi-electron transfer per metal cation (10, 12). The higher melting points ($> 600 \text{ }^\circ\text{C}$) of Mg, Ca, and Al compared to Li, Na, and K ($< 200 \text{ }^\circ\text{C}$) further make multivalent metal batteries attractive in applications requiring compact designs in limited spaces and extreme operation at high temperatures (13, 14).

Following decades of research and development, the field of monovalent and multivalent metal anodes has accumulated impressive knowledge about their electrochemical behaviors in nonaqueous electrolytes. This review aims to compare and contrast their electrochemical commonalities and differences, in terms of metal deposition behaviors, cation solvation structures, and associated electrode-electrolyte interphases. Our main objective is to facilitate knowledge transfer between monovalent and multivalent battery chemistries, and provide insights into unique

design principles and universal development trends for nonaqueous rechargeable Li, Na, K, Mg, Ca, and Al metal batteries.

Comparison of challenges for monovalent and multivalent metals

5 The practical use of monovalent and multivalent metal anodes in rechargeable batteries has long been impeded by two common issues (**Fig. 1A**). The first issue is irregular deposition and dissolution of metal anodes. In a working battery, all monovalent and multivalent cations, irrespective of their chemistry, have a strong tendency to be electrochemically reduced and deposited on the anode surface in irregular, fractal, and even dendritic morphologies during the discharge process (15, 16). Meanwhile, inhomogeneous electrochemical dissolution of metal anode during the charge process generates porous pits and electronically isolated “dead” metal, causing severe capacity loss and safety hazards (17, 18). Another common issue is the high chemical reactivity of metal anodes. The highly negative electrochemical potential of metal anodes (**Fig. 1B**) resides far beyond the thermodynamic stability window of conventional organic electrolytes, as marked by the lowest unoccupied molecular orbitals (LUMOs), driving spontaneous reduction of electrolyte components to form a solid electrolyte interphase (SEI) layer (12, 19). During repeated plating/stripping, mechanical stress from volume fluctuations fractures these typically heterogeneous and fragile SEI. Subsequent exposure of fresh metal triggers perpetual SEI formation through parasitic reactions, accelerating active metal corrosion, gas evolution, and electrolyte depletion (3). This cascade ultimately degrades Coulombic efficiency (CE) and limits cycle life (3).

Beyond their shared commonalities, fundamental differences exist between monovalent and multivalent battery (electro)chemistries stemming from the unique properties of the respective metal anodes and their coupled charge carriers. First, dendrite susceptibility varies with crystal structure. For example, hexagonal close-packed (HCP) Mg and face-centered cubic (FCC) Ca and Al metals exhibit higher surface energies at preferred crystallographic orientations than body-centered cubic (BCC) Li, Na, and K metals, resulting in generally lower tendency for dendrite formation in multivalent metals (**Fig. 1C**) (20). Second, because of their high charge densities (**Fig. 1D**), multivalent cations typically exert large binding energies and strong Coulombic interactions with salt anions and aprotic solvents, which create substantial kinetic barriers to solvated cation migration, cation desolvation, charge transfer, and solid-state diffusion through SEIs (19, 21). Consequently, multivalent systems suffer from high thermodynamic-overpotentials during

plating/stripping, which is in stark contrast to monovalent analogs, where SEIs usually enable kinetically efficient cation transport.

Metal electrodeposition behavior

5 Irregular deposition is a phenomenon inherent to many metal electroplating processes. For Li, Na, and K metal anodes, irregular morphologies, such as whisker-like dendrites, moss-like dendrites, tree-like dendrites, and random spheres (**Fig. 2A-D**) have been widely observed in conventional ether or ester-based electrolytes under moderate conditions (15, 22, 23). Although Mg, Ca, and Al metals are predicted to be non-dendritic anode materials, they do electroplate into
10 detrimental morphologies such as interconnected platelets, aggregates of random fibers/spheres, and tree-like dendrites in some unconventional nonaqueous electrolytes or under extreme conditions (**Fig. 2C-F**) (24-27). Several theoretical models have been proposed to understand the metal electrodeposition behavior. For example, Sand's time model and "space-charge" theory link the growth of dendrite with the distribution of ionic concentration field and electric field at the
15 electrode interface, thus explaining the similar tree-like dendrite deposition behavior when the applied current exceeds the limiting value (J_{lim}) (15, 28). Moreover, Marcus theory predicts that solvent reorganization energy (λ) is larger and exchange current density (j_0) is smaller when the binding strength of the solvent to cations is stronger, which explains why Mg does not form whisker and mossy morphologies whereas Li does (19, 29, 30). Nevertheless, these models and
20 theories are not sufficient in apprehending the dynamic and complicated metal nucleation-growth-dissolution processes in reality, as none of them can fully capture the spectra of environments including deposition substrates (e.g., crystallographic orientations, grain boundaries, natural oxidation films) (18, 31, 32), electroplate conditions (e.g., electrolyte formulations, current densities, deposition capacities) (33-35), and external fields (e.g., stress, temperature, magnetic
25 field, gravity) (24, 27, 36). Therefore, it is important to map the electrodeposition regimes of monovalent and multivalent metals and their evolutionary trends in realistic electrochemical environments.

As fast charging is indispensable for next-generation batteries, many efforts have been devoted to clarifying the relationship between metal deposition morphology and applied current
30 density. At a low current of 0.1 mA cm^{-2} , cryogenic electron microscopy (cryo-EM) observations revealed that most of the deposited Li exhibits a sheet-like, amorphous morphology in a commercial ester-based electrolyte (37). This glassy growth pattern is not limited to Li but has

also been observed in other plating metals such as Na, K, and Mg. As the current increases to 0.5 and further to 2.5 mA cm⁻², the amorphous Li structure changes to a more crystalline and whisker-like structure, indicating that the disorder (amorphous)-order (crystalline) phase transition could be the origin of dendrite growth. However, another study using cryo-EM observed crystalline whisker-like Li deposition at all deposition currents ranging from 0.1 to 9 mA cm⁻² in a similar ester-based electrolyte (38). These contrasting observations prompt further investigation into the relationship between the crystallinity of Li nuclei and the growth of Li whiskers (**Fig. 2A**). As further observed by *in-situ* optical microscopy (OM), the initially formed Li in a wide range of currents (about 1 to 7 mA cm⁻²) are microscopically whisker-like, while their macroscopic morphology is actually mossy (**Fig. 2B**), which resembles typical reaction-limited root growth (39). The chronological imaging further captured a transition from initial mosses to tree-like dendrites (**Fig. 2C**) with a self-amplifying tip growth model when the applied current exceeded the J_{lim} (2.61 mA cm⁻²) while plating time reached the Sand's time (about 2700 s) (39). Nevertheless, the ion-transport limitations alone are insufficient to explain the detrimental Li morphology at relatively high currents (1-10 mA cm⁻²), as it is also influenced by the SEI formed at the Li-electrolyte interface (35). A more recent study further decoupled Li deposition from the SEI influence using an ultramicroelectrode geometry and observed that, independent of electrolyte chemistry and current collector, the distinct Li morphologies all transition to a well-defined (110)-faceted polyhedron at ultrahigh currents up to 1000 mA cm⁻² (22). These studies challenge our previous understanding of Li deposition behavior and highlight the critical interplay between SEI formation and metal growth mechanism.

While metallic Li can endure high rates of discharging and charging (> 20 mA cm⁻²), Na-metal anode exhibits limited reversibility when the current density exceeds 2 mA cm⁻² in analogously commonly used ether-based electrolytes (40). The challenges of fast charging in Na electrodes are exacerbated in conventional ester-based electrolytes, where irregularly isolated hemispherical Na deposits (**Fig. 2D**) lead to short circuits in symmetrical cells after just 5 minutes at 1 mA cm⁻² (23). The short-circuit failure primarily results from the delaminated, irregular Na deposits and fragments from fragile SEIs, and more importantly, their accumulation in the pores of the polymer separator (23, 41). This differs from the Li metal case, where the short-circuit failure is mainly caused by the separator being punctured by Li dendrites. These distinctions primarily arise from the mechanically softer nature of both bulk metallic Na and dendrites as well as the higher solubility of Na-SEI components compared to their Li counterparts (42, 43). However, the soft

characteristics of Na can be somewhat advantageous, as the growth and penetration of Na dendrites can be readily mitigated through optimizing battery stack pressure (42, 44), which has been employed in Li-based batteries (36, 45).

Owing to the combined effects of higher reactivity and lower mechanical modulus of K compared to Li and Na, it is observed that dendrite growth in a K-metal anode causes quicker battery failure (23). Experimentally, irregularly isolated hemispherical K deposition (**Fig. 2D**) is often found even at a low current of 0.01 mA cm^{-2} (46). Intriguingly, elevating the current density to 2 mA cm^{-2} could induce non-dendritic and smooth electroplating, indicating that K dendrites could be healed *in-situ*. This high current density-driven dendrite self-healing phenomenon was first observed in Li batteries, where the internal self-heating promoted self-surface diffusion of Li atoms and self-healing of Li dendrites at current densities above 9 mA cm^{-2} (47). The lower threshold current density with which K dendrites heal compared to Li dendrites can be attributed to the significantly lower energy barriers for self-surface diffusion in K metal (46, 47). These results showcase that customizing battery operating protocols (*e.g.*, controlled high-current pulses) is effective for smoothing dendritic features and improving the safety of fast-charging metal batteries (47).

During galvanostatic Mg electrodeposition, tree-like Mg dendrites similar to those in Li metal batteries were formed in Grignard solutions at 0.921 mA cm^{-2} (48). Whereas “all phenyl” complex (APC) electrolytes enable dense and uniform Mg deposition across $1\text{-}5 \text{ mA cm}^{-2}$, with dendritic protrusions only emerging at 10 mA cm^{-2} (34). Similar to Mg, the electroplating morphologies of Ca also underwent a transition from non-dendritic globules (**Fig. 2D**) to tree-like dendrites (**Fig. 2C**) in a $\text{Ca}(\text{BH}_4)_2/\text{tetrahydrofuran}$ (THF) electrolyte at 20 mA cm^{-2} (49). Combined theoretical calculations, digital modeling, and experimental investigations suggest that the differences in cation desolvation-induced exchange current and deposition substrate properties (*e.g.*, metalphilicity, surface energy, metal-support interaction) are responsible for different J_{lim} at which irregular metal deposition occurs (16, 34, 50). It is noteworthy that, despite being subjected to rigorous current conditions, a dense and flat plating layer was formed on Mg and Ca electrodes before the fractal dendrites began to grow. In other words, there is a diffusion-controlled buffer zone during Mg and Ca deposition, *i.e.*, the applied current exceeds the J_{lim} , but the plating duration is less than the Sand’s time (28, 49). This deposition behavior suggests the potential to safely achieve fast-charging batteries by controlling the current *vs.* capacity, thereby enhancing utilization of divalent metal anodes and beyond in such applications.

In Al metal batteries, various detrimental morphologies, such as tree-like dendrites, pebble stacks, interconnected flakes, and random fibers (**Fig. 2C-F**), have been observed in similar AlCl_3 -based ionic liquid electrolytes at currents around 10 mA cm^{-2} (16, 27). As further monitored by *in-situ* OM, the native surface film of Al_2O_3 was dissolved in the ionic liquid electrolyte, accompanied by the formation of SEI with Al-Cl and Al-O containing species on the anode surface, before protrusions of dendritic Al growth (51). A recently developed molten-salt electrolyte composed of NaCl-KCl-AlCl_3 was observed to enable fast-charging (650 mA cm^{-2}) Al-chalcogen batteries resistant to dendritic shorting at an elevated temperature (*e.g.*, $110 \text{ }^\circ\text{C}$)(13). The insights gained from high working temperatures and advanced electrolyte design provide a perspective for the further development of fast-charging multivalent batteries.

With a more coherent understanding of metal deposition behavior, some effective strategies for dendrite inhibition have been independently established in different battery systems. In particular, it is found that some textured substrates can guide reversible epitaxial electrodeposition of metals along the most close-packed crystal plane *i.e.*, (110) for BCC metals (Li, Na, and K) (52-54), (002) for HCP metals (Mg and Zn) (55, 56), and (111) for FCC metals (Ca and Al) (31). Graphene, with a low lattice mismatch for HCP Zn, could effectively lock Zn electrodeposits into a particular crystallographic orientation, *i.e.*, (002) (56). Based on the lattice matching concept, many substrate materials have been explored for epitaxial electrodeposition of various anode metals (**Fig. 2G-I**), *e.g.*, single-crystal copper (Cu) foils for (110)-textured Li (57); Ti_3C_2 MXene films for (002)-textured Mg (58); gold (Au) nanosheets for (111)-textured Al (56). Significant research progress has also been made in the development of bulk textured metal foils, including (110)-textured Li, (002)-textured Mg, and (111)-textured Al (59-61), and texture exposure of unconventional $(100)_{\text{Li}}$, $(100)_{\text{Na}}$, and $(220)_{\text{Al}}$ planes (62-64). These crystal plane customized metal anodes are capable of enabling sequential pit-less stripping and crack-free plating processes compared to non-texture metal anodes, thereby successfully extending the cycle life of batteries in both liquid and solid electrolytes. While there should be close interplay among the crystalline planes, surface reactivity, SEI formation, deposition/dissolution kinetics, and morphologies, which may also rely on the electrochemically active metal species, the community's understanding remains in infancy.

Cation solvation structure

It is well known that the plating and stripping behavior of metal battery anodes strongly depends on the electrolyte, particularly its solvation structure, as this not only determines the transport of metal cations but also affects the formation of interphases. The solvation structure of electrolytes usually consists of coordination structures formed by working cations (Li^+ , Na^+ , K^+ , Mg^{2+} , Ca^{2+} , and Al^{3+}), solvent molecules, and/or salt anions (**Fig. 3A-G**), depending on the interactions among them. Specifically, the densely charged Mg^{2+} cations and large Ca^{2+} cations seriously diminish the solubility (typically ≤ 0.5 M) of salts with conventional anions, such as bis(trifluoromethane)sulfonimide (TFSI) and trifluoromethanesulfonate (OTF), in ethereal solvents, such as 1,2-dimethoxyethane (DME) (21). Furthermore, the diminished dissociation of salts produces positively charged contact ion-pairs (CIPs, *e.g.*, $[\text{Mg}^{2+}\text{-TFSI}^-]$ and $[\text{Ca}^{2+}\text{-TFSI}^-]$), which preferentially adsorb onto the inner Helmholtz layer and decompose into inorganic-rich and ion-insulating interphases, thereby passivating and deactivating Mg and Ca metal anodes (**Fig. 3B**) (65, 66). In contrast, Li^+ , Na^+ , and K^+ cations are generally solvated by solvent molecules (*e.g.*, DME) in conventional monovalent electrolytes (~ 1.0 M, optimized for maximum conductivity), while most conventional anions (*e.g.*, TFSI $^-$) are excluded from the anode inner Helmholtz layer due to the repulsive force. These solvent-separated ion pairs (SSIPs) usually lead to organic-rich, unstable SEI layers with poor mechanical strength, leading to uncontrollable dendrite formation and rapid battery failure (**Fig. 3A**) (67).

For monovalent metal batteries, current electrolyte design strategies focus on achieving an anion-dominated solvation structure and a robust interfacial layer to suppress dendritic growth. One effective approach is the formulation of high-concentration electrolytes (HCEs) by significantly increasing the salt concentration (typically ≥ 3 M). The high molar ratio of salt to solvent forces anions into the solvation sheath, thereby forming abundant ion pairs and aggregates (AGGs) that contribute to a primarily inorganic SEI (**Fig. 3C**). It is observed that increasing the concentration of lithium bis(fluorosulfonyl)imide (LiFSI) salts in DME triggers the SEI microstructure evolution from a heterogeneous mosaic structure to a homogeneous amorphous structure, accounting for the granular Li electrodeposition with high CE of 99 % (68). Similar electrolyte formulations, such as 5.2 M NaFSI or 4.8 M KFSI in DME, further validate the effectiveness of HCEs in achieving over 99 % reversible Na and K electrodeposition (69, 70). To compensate for the high viscosity and salt cost of HCEs, localized high-concentration electrolytes (LHCEs) have been proposed, in which non-polar diluents are introduced to reduce the salt

concentration to around 1 M while preserving the favorable anion-aggregated solvation structure (Fig. 3D). Among the various reported diluents, some highly fluorinated ethers are demonstrated to be universally suitable for Li, Na, and K-based LHCEs systems (71, 72). A comparative study has found that due to the lower Lewis acidity of K^+ ions, the KFSI-based LHCE showed distinctive metrics over its Li and Na analogs, delivering a higher ion transference number and forming a more dissolution-resistant SEI (72). Another promising approach involves the design of solvent molecules with weak solvation capability so that the anion participates in the cation solvation sheath at low concentrations (around 1 M), known as the weakly solvating electrolyte (WSE) approach (Fig. 3E). Recent efforts have yielded a family of functionalized DME molecules, among which 1,2-diethoxyethane (DEE) with extended terminal alkyl chains, has emerged as a versatile example for preparing Li, Na, and K metal-compatible single-salt-single-solvent (4S) WSEs (73-75). Furthermore, fluoroacetonitrile (FAN), a solvent with small size and low solvation energy selected from a variety of ethereal and carbonate molecules, could formulate a Li 4S WSE (*i.e.*, 1.3 M LiFSI/FA) with previously unknown ion-conduction ligand channel to facilitate fast ion-transport even at $-65\text{ }^\circ\text{C}$ (2). Looking forward, co-solvent or high-entropy LHCEs and WSEs are attractive as next-generation monovalent battery electrolytes, as the high molecular diversity can lead to complementary electrolyte properties and favorable solvation structures (*e.g.*, core-shell, micelle-like, gradient, and oscillatory), creating an anion-derived inorganic-rich interphase while maintaining high ionic conductivity (76, 77).

In the realm of Mg and Ca battery electrolytes, considerable research efforts have been directed toward the creation of solvent-rich solvation structures and the formation of ion-conducting interphases. A notable development is the utilization of strongly solvating solvent molecules, such as dimethylacetamide (DMAc), to promote salt dissociation and interrupt cation-anion coordination in the electrolyte, so that a large number of desirable SSIPs forms in the primary solvation sheath of Mg^{2+} and Ca^{2+} (Fig. 3F) (78, 79). Meanwhile, the 4S strongly solvating electrolytes (SSEs) formulated by combining DMAc molecules with simple $Mg(TFSI)_2$ or $Ca(TFSI)_2$ salts could minimize the undesirable anion decomposition, which results in solvent-derived, inorganic-poor interphases that allow for reversible Mg^{2+}/Mg^0 and Ca^{2+}/Ca^0 redox. Learning from the success of co-solvent strategies in Li, Na, and K electrolytes, these strongly solvating solvent molecules and multidentate methoxyethyl-amine $[-(CH_2OCH_2CH_2N)_n-]$ chelates have also been added into DME-based Mg and Ca electrolyte systems as co-solvents to trigger the reconfiguration of cation solvation structures and enhance the stability and reversibility of divalent

metal anodes (65, 80, 81). However, the overtight cation-solvent coordination in these SSEs results in a high desolvation energy and sluggish charge transport at the liquid-solid interface, thereby limiting further improvement in the reaction kinetics of Mg and Ca metals.

Electrolyte salts are also of great significance to govern the electrolyte solvation structure (82). Substantial efforts are being made not only to utilize commercially available salts in advanced manners (e.g., dual-salt and high-entropy) (83), but also to synthesize new salts through classical chemical reactions (84). Among the newly synthesized weakly coordinating anions, boron cluster anions such as carboranes and fluorinated alkoxy-aluminates/borates stand out as a widely recognized paradigm for the development of monovalent (e.g., Li and Na) and divalent (e.g., Mg, Ca, and Zn) electrolytes (85). Notably, tetrakis(hexafluoroisopropoxy)borate ($[B(\text{hfip})_4]_2$, hfip = $C(\text{H})(\text{CF}_3)_2$) with Mg^{2+} and Ca^{2+} ions in ethereal solvents represents one of the best-performing Mg and Ca electrolytes in terms of decent ionic conductivity ($\sim 8 \text{ mS cm}^{-1}$), high anodic stability ($> 4.0 \text{ V}$), and more attractively, a completely dissociated solvation structure ($\sim 99\%$ of SSIP, **Fig. 3G**) (85, 86). Furthermore, the bulk nature of $B(\text{hfip})_4^-$ is effective in restricting the defluorination decomposition of anions and minimizing the undesired formation of MgF_2 and CaF_2 in electrodeposited Mg and Ca metals ($< 7\%$ atomic percentage) (87). Despite the advances, recent studies reveal that $B(\text{hfip})_4^-$ anions mediate chemical corrosion of divalent metal anodes during calendar aging - a phenomenon warranting further investigation (88). On the other hand, although $\text{Mg}(\text{TFSI})_2/\text{DME}$ and $\text{Ca}(\text{TFSI})_2/\text{DME}$ electrolytes are prone to passivate their respective metallic anodes, they exhibit high anodic stability on Al current collectors probably due to the presence of abundant $[\text{Mg}^{2+}\text{-TFSI}]$ and $[\text{Ca}^{2+}\text{-TFSI}]$ complexes (66, 89). In contrast, monovalent battery electrolytes containing TFSI and FSI anions aggressively corrode Al current collectors when their respective battery operating voltages exceed 4.0 V . This limitation has driven the development of non-corrosive salts featuring asymmetric or cyclic molecular structures to enable high-voltage ($> 4.3 \text{ V}$) and high-energy Li, Na, and K metal batteries (90-92). Nevertheless, the large-scale commercialization of these synthesized salts can be achieved only if the issues of high synthesis cost and insufficient synthetic yield are simultaneously addressed.

In the case of nonaqueous Al metal batteries, efficient electrolytes are mainly mixtures of AlCl_3 and ionic liquids (e.g., 1-ethyl-3-methylimidazolium chloride, $[\text{EMIm}]\text{Cl}$) or Lewis basic ligands (e.g., urea and acetamide) (31, 93, 94). In these ionic liquids, the heterolytic cleavage of AlCl_3 induces the formation of AlCl_4^- , Al_2Cl_7^- species (**Fig. 3H**), and sometimes $[\text{AlCl}_2\cdot(\text{ligand})_n]^+$, which usually allow Al deposition/dissolution to occur reversibly with a high CE $>98\%$.

Meanwhile, organic (*e.g.*, Grignard reagents) and inorganic (*e.g.*, MgCl_2) chlorides are also widely used in Mg electrolyte solutions to generate electrochemically active MgCl^+ and Mg_2Cl_3^+ (**Fig. 3H**), which are beneficial for achieving > 99% reversible Mg electrodeposition (95, 96). However, these metal-chloride complexes in Mg and Al metal batteries not only sacrifice the inherent advantages of Mg/Mg^{2+} and Al/Al^{3+} redox couples, including considerable voltage headroom and multi-electron transfers low redox potentials, but also pose serious corrosion problems for battery components, such as current collectors and casings (16, 54). More efforts are needed to develop chloride-free electrolytes, especially based on simple salts such as $\text{Mg}(\text{TFSI})_2$, $\text{Mg}(\text{OTf})_2$, and $\text{Al}(\text{OTf})_3$ for Mg and Al batteries.

Current work in electrolyte solvation structure modulation also includes the selection of suitable additives, such as multivalent salts (*e.g.*, $\text{Mg}(\text{TFSI})_2$, Al-ethoxide) for Li, Na, or K electrolyte solutions (97, 98) and monovalent salts (*e.g.*, LiOTf , LiBF_4 , NaCl , and KCl) for Mg, Ca, or Al electrolyte solutions (83, 90, 94). Appropriate combinations of additives, salts, and solvents have led to a variety of targeted functionalized electrolytes, such as wide-temperature electrolytes (99), high-voltage electrolytes (76), corrosion-free electrolytes (3, 84), moisture-stable electrolytes (94), and non-flammable electrolytes (75, 82). Further understanding of equilibrium and non-equilibrium structures of cation solvation sheaths, anion-cation pairs, salt-in-salt complexes, molecular clusters, and percolating networks in these advanced electrolytes will bring transformative opportunities to improve electrochemical performance and operation safety of monovalent and multivalent metal batteries beyond their current limitations (1).

Electrode-electrolyte interphase

Located at the nanointerface between the electrode and electrolyte, the SEI's composition and structure strongly depends on initial chemical reactions of metal/electrolytes and continuous electrochemical reduction of electrolytes (100). Using advanced cryo-EM technology, it has recently been disclosed that the SEI layers formed in some nonaqueous Li (6, 101), Na (72, 74), K (54, 72), Mg (102), and Ca (84) electrolytes, are overwhelmingly composed of inorganic (*e.g.*, oxides and fluorides) nanocrystalline domains randomly distributed within organic (*e.g.*, alkoxides) amorphous matrixes, which is largely consistent with the mosaic model (**Fig. 4A**). The heterogeneous mosaic SEIs are shown to cause localized stripping that promotes dendritic and inactive metal formation and early battery failures (103). To stabilize metal-electrolyte interfaces, efforts have been made to improve the physicochemical properties and electrochemical

functionalities of SEIs through optimizing their structural homogeneity and compositional features (5). Nowadays, it is widely accepted that an optimal SEI for monovalent and multivalent metal anodes usually requires similarly thin and homogeneous structures (*e.g.*, multilayer and monolithic structures), yet different inorganic and organic components and their proportions (*e.g.*, organic-rich or inorganic-rich) to achieve some universal advantages, including fast ion transport but negligible electron conduction, a combination of mechanical flexibility and robustness, and selective solubility and minimal swelling in the electrolyte (3, 68, 104).

Enriching the SEI with inorganic components has recently gained popularity in preventing dendritic formation and improving the electrochemical reversibility of Li, Na, and K metal anodes. Compared to conventional inorganic components (*e.g.*, oxides, sulfides), metal fluorides possess some attractive properties, including large bandgap (≥ 10.6 eV for LiF, NaF, and KF), high Young's modulus (~ 65.0 GPa for LiF and 31.4 GPa for NaF), and high interfacial energy (*e.g.*, 73.28 meV \AA^{-2} at the LiF/Li interface), which may prevent electron tunneling at the anode-electrolyte interface and simultaneously boost the growth of deposited metal in a parallel rather than vertical manner (105-108). When these monovalent fluorides are homogeneously interfaced with other inorganic ingredients, the resulting hybrid SEI layers (*e.g.*, LiF/Li₂O/Li₂ZrF₆, NaF/Na₂O/Na₂CO₃, KF/K₂CO₃/K₃PO₄) feature microstructures abundant in grain boundaries, which can promote rapid interfacial ion transport and inhibit unwanted SEI reformation/swelling during cycling (72, 74, 108). However, despite the high mechanical modulus of these fluorinated inorganic-rich SEIs, their mechanical conformality is normally questionable in safeguarding long-term interfacial integrity and cycling stability of metal anodes, which are subjected to continuous volumetric deformation (5). On the other hand, organic SEI components, especially some elastomers and viscoelastic polymers, such as poly(vinylidene fluoride) (PVDF), poly(1,3-dioxolane) (PDOL), and poly(tetrafluoroethylene) (PTFE), are highly flexible to buffer the tensile and compressive stress during repeated plating and stripping processes. Therefore, a series of fluorinated inorganic/organic hybrid SEIs (*e.g.*, LiF/PVDF, NaF/PDOL/graphene oxide, KF/PTFE) have been constructed to simultaneously improve the interfacial kinetics and stability of Li, Na, and K metal anodes (109-111). In particular, a bilayer SEI (**Fig. 4B**), consisting of a LiF-rich inner layer and an outer layer containing lithium polyoxymethylene (LiPOM), has been shown to offer advantages over a single-layer LiF-rich SEI by enabling an extended lifespan of high-energy Li metal batteries (430 cycles *vs.* 200 cycles) (5). In addition to qualitatively engineering fluorinated SEI chemistry, research progress has also been made in accurately

quantifying and identifying the specific interphase components (*e.g.*, LiF, Li₂O, LiH, and NaH), visualizing their spatial locations in dendrites and/or SEIs, tracking their chemical origin, and determining their relation with inactive metal (*e.g.*, Li and Na) formation as well as battery reversibility (112-115).

5 Early studies on the SEI in multivalent metal batteries suggest that decreasing ion-resistive inorganics such as MgF₂, CaF₂, and Al₂O₃, while increasing ion-conductive organic components, is critical to unlock the reversible plating/stripping cycling of Mg, Ca, and Al metal anodes (81, 84). In Mg metal batteries, one of the most notable organic-rich SEIs was *ex-situ* made from thermal-cyclized polyacrylonitrile (cPAN) and Mg(OTf)₂ salts, which not only permits Mg²⁺ transport at a moderate ionic conductivity of 1.19×10⁻⁶ S cm⁻¹, but also enables efficient and reversible Mg²⁺/Mg⁰ redox reactions in Mg(TFSI)₂-based carbonate electrolytes (116). In parallel, the *in-situ* generation of SEI layers rich in poly(tetrahydrofuran) and B-O cross-linked polymer was also demonstrated to be conducive to non-passivating and dendrite-free Mg deposition with a high average CE > 98% (81, 117). Similarly, in Ca metal batteries, an organoboron-rich and CaF₂-poor SEI layer derived from additive-regulated Ca(TFSI)₂-based electrolytes was capable of permitting active percolation of Ca²⁺, rather than inducing passivation on the Ca metal anode (**Fig. 4C**) (118). Furthermore, in Al metal battery systems, an SEI layer predominantly composed of C=C and C=O species was artificially introduced to replace the natural passivation Al₂O₃ layer on Al metal, thus aiding in its reversible stripping/deposition in Al(OTf)₃-based electrolytes (119).
10
15
20 Despite these advances, the precise chemical composition and ion-conducting mechanisms of these organic-rich SEI layers are still poorly understood due to their amorphous nature.

While multivalent oxides and fluorides are traditionally considered cation-insulating components (100, 120), this notion has been challenged by recent studies showing that some thin MgO/MgF₂, AlF₃-rich bilayers, or CaF₂-rich mosaic interphases could also work as SEI layers to permit fast ion conduction in Mg(TFSI)₂, Al(OTf)₃, or Ca(TFSI)₂ based nonaqueous electrolytes (14, 121, 122). In contrast to the conflicting roles of multivalent fluorides, other inorganic chlorides (MgCl₂, AlCl₃), bromides (MgBr₂, CaBr₂), iodides (MgI₂, CaI₂), and especially hydrides (MgH₂, CaH₂) have been widely studied as beneficial SEI components for multivalent metal anodes due to their low ion diffusion barriers (79, 120, 123). A thin (~ 5 nm) and monolithic SEI layer enriched with MgH₂ species (**Fig. 4C**), enabled by the synergy between the coordination and trace ionization of amine cosolvents, was conducive to inducing Mg²⁺ rapid transfer and uniform deposition in Mg(TFSI)₂-based electrolytes (124). In addition, metallic Ca electrodeposited in the
25
30

organoborate electrolytes was covered by a conformable SEI layer with high concentrations of amorphous Ca-H_x species, contributing to highly reversible and long-life Ca metal batteries (84). These studies challenge our previous understanding of the existence and role of interphase layers in multivalent metal batteries and highlight the importance of the thickness and structure of SEI layers, alongside their chemical composition and crystallinity, in determining the ion transport behavior at electrified electrode-electrolyte interfaces.

For monovalent and multivalent metals, research efforts have also been devoted to introducing foreign metal compounds into their respective SEI layers to build optimal electrode-electrolyte interfaces with fast interfacial kinetics and efficient dendrite suppression. One example of this is the development of alloy/halide biphasic mixed conductive interphases, which combine the high metal affinity and ionic diffusivity of metal alloys with the high mechanical strength and electrochemical stability of metal halides. The effectiveness of alloy/halide biphasic SEI layers was first demonstrated in Li metal anodes such as Li₁₃In₃/LiCl (125), and successfully extended to Na, K, Mg, Ca, and Al metal anodes such as Na-Sn/NaF, K-Bi/K₃OCl, Mg-Sb/MgCl₂, Ca-Sn/CaI₂, and Al-Bi/AlCl₃ (79, 126-129). In the case of Li metal batteries, a series of protective layers consisting of Li-M (M=Mg, Ca, Al)/LiF were built via two-step replacement and alloying reactions between Li metal anodes and multivalent electrolyte additives (MgF₂, CaF₂, and AlF₃) (Fig. 4D) (130). In contrast, the addition of monovalent salts (LiCl, NaCl, and KCl) in the ionic liquid electrolytes of Al metal battery systems resulted in the formation of hybrid cation salts (e.g., Na_xAl_yO₂) rather than alloy (e.g., Na-Al) in the SEI layers (Fig. 4E) (93). These differences arise from the distinct electrode potentials between multivalent and monovalent metals, where Mg²⁺, Ca²⁺, and Al³⁺ can be reduced on the monovalent metals, but Li⁺, Na⁺, and K⁺ cannot be reduced on the multivalent metals. More interestingly, it has been found that a Li-species-containing SEI layer could enable stable reversible Mg and Ca plating/stripping in Mg(TFSI)₂ and Ca(TFSI)₂ based electrolytes (98, 131), while the Mg-species-containing inactive passivating layer could transform into an active and robust interphase for Li metal anodes (96). Nevertheless, research on hybrid cation SEI is still at an early stage, and more systematic and in-depth studies are needed to clarify the similarities and differences in their working mechanisms in monovalent and multivalent batteries.

Besides Li, Na, K, Mg, Ca, Al-containing compounds, many other functional materials such as MXenes, and metal-organic frameworks have been used to construct compositionally optimized, structurally homogeneous, and mechanically stable SEI layers either *in-situ* or *ex-situ* (132). While

most of these SEI layers are efficient in stabilizing electrode surface and improving ion diffusion at the electrode/electrolyte interface, they are unable to provide effective and sufficient ion-conducting channels to the massive bulk metal inside the electrodes, which typically have a thickness greater than 100 μm . Recently, thin composite metal electrodes have demonstrated potential in tackling these problems, as they can be easily manufactured through industry-compatible high-temperature melting and mechanical rolling processes and form built-in interconnected conductive interphases embedded with bulk active metal. Composite metal electrodes mainly include alloys, such as Li/Li₂₂Sn₅, Ca₂Sn, and AZ31 Mg (3% Al, 1% Zn by weight) (86, 133, 134), and “salt-in-metal” foils, such as Li/SnF₂, Li/zinc dialkyldithiophosphate (ZDDP), Na/Sb-SnO₂, and K/Bi₂Te₃ (63, 105, 135, 136). These composite electrodes possess significant advantages over pure metal electrodes, including fast ionic diffusion capabilities throughout the entire electrode, homogeneous stripping and plating processes, suppressed galvanic corrosion at grain boundaries, enhanced thermal stability at high temperatures, or strengthened interfacial compatibility with liquid and solid electrolytes. Together with their thin thickness, some composite electrodes, such as $\leq 20 \mu\text{m}$ for Li/ZDDP and $25 \mu\text{m}$ for AZ31 Mg, hold great promise in simultaneously improving the energy density and cycling stability of monovalent and multivalent metal batteries (134, 136).

Nowadays, researchers have found that the SEI chemistry depends not only on the electrolyte solvates at the electrified electrode-electrolyte nanointerface, but also on multiple components in an actual battery, such as cathode (*e.g.*, cross-talk of transition metal ions and shuttling effect of polysulfides species), separator (*e.g.*, chemical reactions between glass fiber and Al deposits), and current collector (especially for anode-free battery configuration). Furthermore, the decomposition of electrolyte solvents (*e.g.*, DME and amines) and contaminants (*e.g.*, moisture) may release gas byproducts (*e.g.*, CH₄ and H₂), which not only can react with Li, Na, or Mg metal to produce extended H-species-containing interphases, but also disrupt ion and electron transport paths, resulting in irregular metal deposition (102, 115, 137). Meanwhile, the dissolution and reformation of SEI have been widely observed in monovalent and multivalent batteries, but their impact on battery cyclability is embroiled in controversy. While it is widely accepted that SEI dissolution is a major contributor to anode corrosion and associated with interface instability, capacity loss, and battery self-discharge, some experimental observations evidence the positive role of SEI dissolution in leaching detrimental moisture and chloride species from Mg batteries (138), and enhancing the content and distribution of LiF and NaF on Li and Na electrode surface

(3, 43, 105). Overall, it remains a great challenge to decipher and manage the morphological and structural evolution of initially designed fluorinated inorganic-rich SEI for Li, Na, and K as well as hydrogenated organic-rich SEI for Mg and Ca during battery aging, formation, conditioning, and cycling processes.

5

Outlook

Over the last decade, there has been a significant surge in research focused on battery chemistry and materials, with a notable emphasis on metal anodes. While considerable progress has been made in understanding and tailoring monovalent and multivalent metal anodes, some critical knowledge regarding their electrochemical plating/stripping behaviors is still missing, including but not limited to (i) the real-time structural, chemical, and morphological information of the electrodeposited metal at the nanometer- or micrometer-scale; (ii) the temporal and spatial transformation from the electrolyte into interphases at the electrified liquid-solid interface (iii) the complex interactions among electrodeposited metals, electrolyte solvates, and interphase components, and their precise correlation with electrode reversibility. In the field of Li metal anodes, new insights are being offered by various advanced *in-situ/operando* characterization tools, non-destructive diagnosing techniques, multi-modality analysis approaches, and powerful supercomputing sources. For example, *in-situ* liquid-phase transmission electron microscopy (TEM) and electrified cryo-EM have enabled direct observation of particle growth patterns in the early stages of Li⁺ plating and quantification of the two-stage growth of SEI in a Li-based tweezer battery, respectively (139, 140). By collecting electrolyte datasets from *operando* spectroscopy, *ab initio* molecular dynamics (AIMD) simulations, and density functional theory (DFT) calculations, as well as building machine learning (ML) models and molecular universes based on them, researchers found that besides cation-anion aggregates/solvates, both electrolyte dielectric environment and solvent oxygen ratio are also critical descriptors controlling interphase chemistry and Li plating/stripping reversibility (67, 141). Quantitative analysis of the cycled Li anode using titration gas chromatography, ultrasonic imaging, and morphological characterization revealed that the loss of lithium inventory is more complex than previously thought, involving the contribution of electronically isolated and ionically isolated Li metal generated under coupled electro-chemical-mechanical fields (45, 112). Similar systematic, quantitative, and comparative investigations are beginning to appear in the field of Na, K and Mg battery anodes (44, 72, 115,

10

15

20

25

30

142), and we encourage more of such efforts to expand our fundamental understanding of the electrochemical commonalities and differences between monovalent and multivalent metal anodes.

The ultimate success of metal anodes in commercial batteries hinges on addressing both scientific and technical challenges while leveraging their unique metrics for specific applications.

5 Owing to the synergies of Li metal-compatible electrolyte solutions (*e.g.*, HCEs, LHCEs, and WCEs), advanced manufacturing processes (*e.g.*, 20 μm Li metal foil anode), and/or suitable battery configurations (*e.g.*, anode-free), researchers have succeeded in making $> 500 \text{ Wh kg}^{-1}$ Li metal pouch batteries (7), and commercial sectors are actively pursuing LMB applications in electric vehicles and electric aviation (11, 143). Future efforts should be dedicated to improving battery longevity and safety under fast charging (1C to 5C as recommended by the Advanced Battery Coalition of the United States), low stacking pressure (ideally $< 700 \text{ kPa}$), extreme temperatures ($-80 \text{ }^\circ\text{C}$ to $80 \text{ }^\circ\text{C}$), and industrial abuses (short-circuiting, nail penetration, and crushing)(11). Although solid-state electrolytes have emerged as a promising choice to ensure high battery safety, they still encounter inherent limitations including poor interfacial contact, dendrite propagation, and Li metal anode fatigue (144). In the near future, data-driven and/or knowledge-driven design of additives that work synergistically with aggregate-dominated electrolytes and fluorinated inorganic-rich interphases remains an attractive path forward. In the meantime, reactivating isolated inactive Li metal and introducing external Li supplies also provide transformative opportunities for reshaping Li loss and increasing the lifetime of batteries (145, 146).

20 Learning from the commonalities and differences with Li-based battery chemistry, both academia and industry have witnessed significant advances in Na and K metal batteries. The energy density of Na and K metal batteries has been increased to over 200 Wh kg^{-1} at the cell level and 400 Wh kg^{-1} at the material level in anode-free configurations, respectively (147, 148). In addition to maximizing specific energy, the anode-free design also avoids the handling of metallic Na and K electrodes, which are unstable even in dry room conditions, and allows the use of Al foil as anode current collectors, which differs from Cu foils typically used in Li batteries. Specifically, calculations have indicated that replacing Cu with Al and Li with Na (or K) can reduce overall costs, where the implicit cost of Cu-Al replacement is 2.3 times that of Li-Na (or K) replacement (50). Despite their considerable energy density at low expected cost, the cycle life of Na and K-based battery technologies is still far from the requirements (> 1000 charge-discharge cycles) for grid-scale stationary energy storage, and for starting, lighting, and ignition batteries. To prolong

the battery longevity beyond current limits, further research efforts should focus on inexpensive Al current collectors, including engineering microstructures and crystal planes for uniform and dense Na/K deposition, as well as tailoring surface reactivity and electrolyte formulations for homogeneous and stable Na/K interphase formation.

5 Multivalent metal-based battery chemistries are still at the basic research and development stage. The cell-level energy density of state-of-the-art Mg (53.4 Wh kg^{-1}) and Al (90.1 Wh kg^{-1}) metal batteries is far inferior to that of today's LIBs, and the prototype of Ca metal pouch batteries was only demonstrated recently (84, 88, 149). Nevertheless, it is estimated that the specific energy can be further improved to $>150 \text{ Wh kg}^{-1}$ when thin metal electrodes (e.g., $20.8 \mu\text{m}$ Mg, $38.4 \mu\text{m}$ Ca, and $9.6 \mu\text{m}$ Al) are employed to match high-loading cathodes (industry standards typically exceed 4.0 mAh cm^{-2}) with limited negative/positive (N/P) ratios (generally ≤ 2) (149, 150). Note that the anode-free configuration may not be easily adaptable for multivalent metal batteries, as most cathode materials (e.g., Mo_6S_8 , MnO_2 , graphite) do not contain Mg, Ca, or Al and are in a charged state (58), unlike the typical cathode materials (e.g., LiFePO_4 , Na-TMO, K-Prussian blue) of monovalent metal batteries, which are in an initially discharged state. More importantly, anode-free multivalent battery technologies may overlook the advantages of Mg, Ca, and Al metal anodes compared to Li, Na, and K counterparts, including air stability, high-temperature stability, and metallurgical properties. These properties position multivalent metal batteries for extreme applications like high-temperature ($> 100 \text{ }^\circ\text{C}$) or flexible textile batteries (13, 14). We hope that our comparison between monovalent and multivalent metal anodes will help electrochemists and material scientists in the rational design of electrodes, electrolytes, and their interfaces for the coming-generation Mg, Ca, and Al metal batteries and beyond. We also encourage researchers from mechanical engineering, metallurgy, automotive manufacturing, and many other fields, to participate in the battery industry, eventually accelerating the electrification of modern society and realizing our low-carbon future.

References and Notes

1. Y. S. Meng, V. Srinivasan, K. Xu, Designing better electrolytes. *Science* **378**, 1065 (2022).
2. L. Li *et al.*, Ligand-channel-enabled ultrafast Li-ion conduction. *Nature* **627**, 101-107 (2024).
3. H. Kwon *et al.*, Borate-pyran lean electrolyte-based Li-metal batteries with minimal Li corrosion. *Nat. Energy* **9**, 57-69 (2024).
4. Y. Jie *et al.*, Towards long-life 500 Wh kg^{-1} lithium metal pouch cells via compact ion-pair aggregate electrolytes. *Nat. Energy* **9**, 987-998 (2024).

5. Q.-K. Zhang *et al.*, Homogeneous and mechanically stable solid-electrolyte interphase enabled by trioxane-modulated electrolytes for lithium metal batteries. *Nat. Energy* **8**, 725-735 (2023).
6. Y. Liu *et al.*, Self-assembled monolayers direct a LiF-rich interphase toward long-life lithium metal batteries. *Science* **375**, 739-774 (2022).
7. Q. Li, Y. Yang, X. Yu, H. Li, A 700 W·h·kg⁻¹ Rechargeable Pouch Type Lithium Battery. *Chinese Phy. Lett.* **40**, 048201 (2023).
8. K. Kakiage, T. Yano, H. Uehara, M. Kakiage, Ultra-lightweight rechargeable battery with enhanced gravimetric energy densities >750 Wh kg⁻¹ in lithium-sulfur pouch cell. *Commun Eng.* **3**, 177 (2025).
9. Z. Wen, Y. Liu, K. Li, S. Yang, H. Zhou, P. He, Boosting the Li-O₂ pouch cell beyond 860 Wh kg⁻¹ with an O₂-enriched localized high-concentration electrolyte. *Nat. Sci. Rev.* **12**, nwaf059 (2025).
10. G. Rayner-Canham, T. Overton, **Descriptive Inorganic Chemistry**, 5th ed., W. H. Freeman and Company, New York, 2009.
11. G. Brunklaus, P. Lennartz, M. Winter. Metal electrodes for next-generation rechargeable batteries. *Nat. Rev. Ele. Eng.* **1**, 79-92 (2024).
12. H. Zhang *et al.*, From lithium to emerging mono- and multivalent-cation-based rechargeable batteries: non-aqueous organic electrolyte and interphase perspectives. *Energy Environ. Sci.* **16**, 11-52 (2023).
13. Q. Pang *et al.*, Fast-charging aluminium-chalcogen batteries resistant to dendritic shorting. *Nature* **608**, 704-711 (2022).
14. L. Ye *et al.*, A rechargeable calcium-oxygen battery that operates at room temperature. *Nature* **626**, 313-318 (2024).
15. H. Liu, *et al.*, Recent advances in understanding dendrite growth on alkali metal anodes. *EnergyChem* **1**, 100003 (2019).
16. Y. Liang, H. Dong, D. Aurbach, Y. Yao, Current status and future directions of multivalent metal-ion batteries. *Nat. Energy* **5**, 646-656 (2020).
17. X. Liu *et al.*, Uneven Stripping Behavior, an Unheeded Killer of Mg Anodes. *Adv. Mater.* **34**, 2201886 (2022).
18. M. Baek *et al.*, Naked metallic skin for homo-epitaxial deposition in lithium metal batteries. *Nat. Commun.* **14**, 1296 (2023).
19. X. Chen *et al.*, Ion-Solvent Chemistry-Inspired Cation-Additive Strategy to Stabilize Electrolytes for Sodium-Metal Batteries. *Chem* **6**, 2242-2256 (2020).
20. K. S. Nagy, S. Kazemiabnavi, K. Thornton, and D. J. Siegel. Thermodynamic overpotentials and nucleation rates for electrodeposition on metal anodes. *ACS Appl. Mater. Interfaces* **11**, 7954-7964 (2019).
21. J. Kim *et al.*, Insights from Li and Zn systems for advancing Mg and Ca metal batteries. *Chem. Soc. Rev.* **53**, 8878 (2024).
22. X. Yuan, B. Li, M. Mecklenburg, Y. Li, Ultrafast deposition of faceted lithium polyhedra by outpacing SEI formation. *Nature* **620**, 86-91 (2023).
23. J. Hu *et al.*, Electrochemical deposition mechanism of sodium and potassium. *Energy Storage Mater.* **36**, 91-98 (2021).
24. R. Davidson *et al.*, Mapping mechanisms and growth regimes of magnesium electrodeposition at high current densities. *Mater. Horiz.* **7**, 843-854 (2020).
25. J. Eaves-Rathert, K. Moyer, M. Zohair, C. L. Pint, Kinetic- versus diffusion-driven three dimensional growth in magnesium metal battery anodes. *Joule* **4**, 1324-1336 (2020).

26. D. Wang *et al.*, Plating and stripping calcium in an organic electrolyte. *Nat. Mater.* **17**, 16-20 (2018).
27. D. Pradhan, R. G. Reddy, Dendrite-Free Aluminum Electrodeposition from AlCl₃-1-Ethyl-3-Methyl-Imidazolium Chloride Ionic Liquid Electrolytes. *Metall. Mater. Trans. B* **43**, 519-531 (2012).
28. X. Liu *et al.*, A perspective on uniform plating behavior of Mg metal anode: diffusion limited theory versus nucleation theory. *Adv. Mater.* **36**, 2306395 (2023).
29. M. Jäckle, K. Helmbrecht, M. Smits, D. Stottmeisterab, A. Groß, Self-diffusion barriers: possible descriptors for dendrite growth in batteries? *Energy Environ. Sci.* **11**, 3400-3407 (2018).
30. D. T. Boyle *et al.*, Transient Voltammetry with Ultramicroelectrodes Reveals the Electron Transfer Kinetics of Lithium Metal Anodes. *ACS Energy Lett.* **5**, 701-709 (2020).
31. J. Zheng *et al.*, Regulating electrodeposition morphology in high-capacity aluminium and zinc battery anodes using interfacial metal-substrate bonding. *Nat. Energy* **6**, 398-406 (2021).
32. P. Shi *et al.*, Inhibiting intercrystalline reactions of anode with electrolytes for long-cycling lithium batteries. *Sci. Adv.* **8**, eabq3445 (2022).
33. Z. Liu *et al.*, Dendrite-free Lithium Based on Lessons Learned from Lithium and Magnesium Electrodeposition Morphology Simulations. *Cell Rep. Phy. Sci.* **2**, 100294 (2021).
34. J. H. Kwak *et al.*, Operando Visualization of Morphological Evolution in Mg Metal Anode: Insight into Dendrite Suppression for Stable Mg Metal Batteries. *ACS Energy Lett.* **6**, 162-170 (2021).
35. D. T. Boyle *et al.*, Resolving current-dependent regimes of electroplating mechanisms for fast charging lithium metal anodes. *Nano Lett.* **22**, 8224-8232 (2022).
36. C. Fang *et al.*, Pressure-tailored lithium deposition and dissolution in lithium metal batteries. *Nat. Energy* **6**, 987-994 (2021).
37. X. Wang *et al.*, Glassy Li metal anode for high-performance rechargeable Li batteries. *Nat. Mater.* **19**, 1339-1345 (2020).
38. Y. Xu, H. Wu, H. Jia, J.-G. Zhang, W. Xu, C. Wang, Current density regulated atomic to nanoscale process on Li deposition and solid electrolyte interphase revealed by cryogenic transmission electron microscopy. *ACS Nano* **14**, 8766-8775 (2020).
39. P. Bai, J. Li, F. R. Brushetta, M. Z. Bazant, Transition of lithium growth mechanisms in liquid electrolytes. *Energy Environ. Sci.* **9**, 3221-3229 (2016).
40. Y. Zhong *et al.*, Mechanistic Insights into fast charging and discharging of the sodium metal battery anode: a comparison with lithium. *J. Am. Chem. Soc.* **143**, 13929-13936 (2021).
41. K. C. Matthews, B. Rush, R. Gearba, X. Guo, G. Yu, J. H. Warner, Cryo-Electron Microscopy Reveals Na Infiltration into Separator Pore Free-Volume as a Degradation Mechanism in Na Anode:Liquid Electrolyte Electrochemical Cells. *Adv. Mater.* **36**, 2308711 (2024).
42. W. Jiao *et al.*, Critical Role of Pressure for Chemo-Mechanical-Induced Stability of Sodium Metal Battery Anodes. *ACS Energy Lett.* **8**, 2711-2717 (2023).
43. X. Guo, *et al.*, Interface-Compatible Gel-Polymer Electrolyte Enabled by NaF Solubility-Regulation toward All-Climate Solid-State Sodium Batteries. *Angew. Chem. Int. Ed.* **63**, e202402245 (2024).
44. B. Sayahpour *et al.*, Quantitative analysis of sodium metal deposition and interphase in Na metal batteries. *Energy Environ. Sci.* **17**, 1216-1228 (2024).
45. X. Duan *et al.*, Revealing ionically isolated Li loss in practical rechargeable Li metal pouch

cells. *Sci. Bull.* **70**, 914-922 (2025).

46. P. Hundekar *et al.*, In situ healing of dendrites in a potassium metal battery. *Proc. Natl. Acad. Sci. U.S.A.* **117** 5588-5594 (2020).
47. L. Li *et al.*, Self-heating-induced healing of lithium dendrites. *Science* **359**, 1513-1516 (2018).
48. R. Davidson *et al.*, Formation of Magnesium Dendrites during Electrodeposition. *ACS Energy Lett.* **4**, 375-376 (2018).
49. S. D. Pu *et al.*, Current-density-dependent electroplating in Ca electrolytes: from globules to dendrites. *ACS Energy Lett.* **5**, 2283-2290 (2020).
50. G. Zou *et al.*, A nanotwinned-alloy strategy enables fast sodium deposition dynamics. *Nat. Commun.* **16**, 1795 (2025).
51. Y. Long *et al.*, Suppressing Al dendrite growth towards a long-life Al-metal battery. *Energy Storage Mater.* **34**, 194-202 (2021).
52. H. Chen *et al.*, Synthesis of monocrystalline lithium for high-critical-current-density solid-state batteries. *Nat. Synth.* **4**, 552-561 (2025).
53. J. Wang *et al.*, A sodiophilic amyloid fibril modified separator for dendrite-free sodium-metal batteries. *Adv. Mater.* **36**, 2304942 (2024).
54. X. Lian *et al.*, An electric double layer regulator empowers a robust solid-electrolyte interphase for potassium metal batteries. *Energy Environ. Sci.* **18**, 322-333 (2025).
55. G. Yang *et al.*, Realizing horizontal magnesium platelet deposition and suppressed surface passivation for high-performance magnesium metal batteries. *Energy Environ. Sci.* **17**, 1141-1152 (2024).
56. J. Zheng *et al.*, Reversible epitaxial electrodeposition of metals in battery anodes. *Science* **366**, 645-648 (2019).
57. M.-H. Kim *et al.*, Horizontal lithium growth driven by surface dynamics on single crystal Cu(111) foil. *Energy Environ. Sci.* **17**, 6521-6532 (2024).
58. Y. Li *et al.*, MXene-based anode-free magnesium metal battery. *Adv. Funct. Mater.* **33**, 2303067 (2023).
59. J. Tan *et al.*, Scalable Customization of Crystallographic Plane Controllable Lithium Metal Anodes for Ultralong-Lasting Lithium Metal Batteries. *Adv. Mater.* **36**, 2403750 (2024).
60. S. Wang *et al.*, Preferred crystal plane electrodeposition of aluminum anode with high lattice-matching for long-life aluminum batteries. *Nat. Commun.* **15**, 6476 (2024).
61. J. Bi *et al.*, Enhancing Reversibility and Stability of Mg Metal Anodes: High-Exposure (002) Facets and Nanosheet Arrays for Superior Mg Plating/Stripping. *Angew. Chem. Int. Ed.* **63**, e202407770 (2024).
62. J. Zheng *et al.*, Textured Electrodes: Manipulating Built-In Crystallographic Heterogeneity of Metal Electrodes via Severe Plastic Deformation. *Adv. Mater.* **34**, 2106867 (2021).
63. Z. Li *et al.*, Na (100)-Textured Electrode Embedded with Sb-Doped SnO₂ Nanoparticles for Dendrite-Free Sodium Metal Batteries. *Adv. Energy Mater.* **14**, 2402284 (2024).
64. M. Zhang *et al.*, Selective facet etching enables dendrite-less molten salt aluminum metal batteries. *Nat. Sci. Rev.* **12**, nwaf233, (2025).
65. S. Hou *et al.*, Solvation sheath reorganization enables divalent metal batteries with fast interfacial charge transfer kinetics. *Science* **374**, 172-178 (2021).
66. C. Li, R. D. Guha, A. Shyamsunder, K. A. Persson, L. F. Nazar, A weakly ion pairing electrolyte designed for high voltage magnesium batteries. *Energy Environ. Sci.* **17**, 190-201 (2024).
67. S. Zhang *et al.*, Oscillatory solvation chemistry for a 500 Wh kg⁻¹ Li-metal pouch cell. *Nat. Energy* **9**, 1285-1296 (2024).

68. Y. Chen *et al.*, Origin of dendrite-free lithium deposition in concentrated electrolytes. *Nat. Commun.* **14**, 2655 (2023).
69. J. Zheng, S. Chen, W. Zhao, J. Song, M. H. Engelhard, J.-G. Zhang, Extremely Stable Sodium Metal Batteries Enabled by Localized High-Concentration Electrolytes. *ACS Energy Lett.* **3**, 315-321 (2018).
- 5 70. P. Gao *et al.*, Ultrastable dendrite-free potassium metal batteries enabled by weakly-solvated electrolyte. *ACS Nano* **17**, 20325-20333 (2023).
71. X. Che, L. Qin, J. Sun, S. Zhang, D. Xiao, Y. Wu, Phase transfer-mediated degradation of ether-based localized high-concentration electrolytes in alkali metal batteries. *Angew. Chem. Int. Ed.* **61**, e202207018 (2022).
- 10 72. L. Wang *et al.*, Superior electrochemical performance of alkali metal anodes enabled by milder Lewis acidity. *Energy Environ. Sci.* **17**, 3470-3481 (2024).
73. I. R. Choi *et al.*, Asymmetric ether solvents for high-rate lithium metal batteries. *Nat. Energy* **10**, 365-379 (2025).
- 15 74. S. Wang *et al.*, Unraveling the Solvent Effect on Solid-Electrolyte Interphase Formation for Sodium Metal Batteries. *Angew. Chem. Int. Ed.* **62**, e202313447 (2023).
75. X. Yi *et al.*, Safe electrolyte for long-cycling alkali-ion batteries. *Nat. Sustain.* **7**, 326-337 (2024).
- 20 76. S. C. Kim *et al.*, High-entropy electrolytes for practical lithium metal batteries. *Nat. Energy* **8**, 814-826 (2023).
77. W. Chen *et al.*, Hybrid solvating electrolytes for practical sodium metal batteries. *Joule* **9**, 101811 (2025),
78. Z. Hou *et al.*, Correlation between electrolyte chemistry and solid electrolyte interphase for reversible Ca metal anodes. *Angew. Chem. Int. Ed.* **61**, e202214796 (2022).
- 25 79. J. Liang *et al.*, Corrosion of Calcium Metal in Ca(TFSI)₂/DMAc Electrolyte and its Solution via Alloy Interface and Competitive Solvation. *Angew. Chem. Int. Ed.* **64**, e202502729 (2025).
80. H. Dong *et al.*, High-power Mg batteries enabled by heterogeneous enolization redox chemistry and weakly coordinating electrolytes. *Nat. Energy* **5**, 1043-1050 (2020).
- 30 81. Y. Sun *et al.*, Non-nucleophilic electrolyte with non-fluorinated hybrid solvents for long-life magnesium metal batteries. *Energy Environ. Sci.* **16**, 265-274 (2023).
82. J. He *et al.*, Tuning the solvation structure with salts for stable sodium-metal batteries. *Nat. Energy* **9**, 446-456 (2024).
83. S. Wang *et al.*, High-entropy Electrolyte Enables High Reversibility and Long Lifespan for Magnesium Metal Anodes. *Angew. Chem. Int. Ed.* **62**, e202304411 (2023).
- 35 84. S. Li *et al.*, Cation replacement method enables high-performance electrolytes for multivalent metal batteries. *Nat. Energy* **9**, 285-297 (2024).
85. T. Mandai, H. Naya, H. Masu, Comparative studies on [B(HFIP)₄]-based electrolytes with mono- and divalent Cations. *J. Phy. Chem. C* **127**, 7987-7997 (2023).
- 40 86. Z. Zhao-Karger *et al.*, Calcium-tin alloys as anodes for rechargeable non-aqueous calcium-ion batteries at room temperature. *Nat. Commun.* **13**, 3849 (2022).
87. P. Jankowski *et al.*, Development of Magnesium Borate Electrolytes: Explaining the Success of Mg[B(hfip)₄]₂ Salt. *Energy Storage Mater.* **14**, 1133-1143 (2022).
88. H. Lin *et al.*, Deciphering the dynamic interfacial chemistry of calcium metal anodes. *Energy Environ. Sci.* **17**, 6548-6558 (2024).
- 45 89. S. Yang *et al.*, Revisiting the interfacial chemistry of calcium metal anodes: the importance of inorganic-rich solid/electrolyte interfaces derived from an aggregation-dominated electrolyte. *Energy Environ. Sci.* **18**, 1941-1951 (2025).

90. Y. Xia *et al.*, Designing an asymmetric ether-like lithium salt to enable fast-cycling high-energy lithium metal batteries. *Nat. Energy* **8**, 934-945 (2023).
91. A.-M. Li, P. Y. Zavalij, F. Omenya, X. Li C. Wang, Salt-in-presalt electrolyte solutions for high-potential non-aqueous sodium metal batteries. *Nat. Nanotechnol.* **20**, 388-396 (2025).
- 5 92. Y. Hu *et al.*, Cyclic-anion salt for high-voltage stable potassium-metal batteries. *Natl. Sci. Rev.* **9**, nwac134 (2022).
93. M. C. Lin *et al.*, An ultrafast rechargeable aluminium-ion battery. *Nature* **520**, 325-328 (2015).
94. C. Xu, T. Diemant, X. Liu, S. Passerini, Modified Solid Electrolyte Interphases with Alkali Chloride Additives for Aluminum-Sulfur Batteries with Enhanced Cyclability. *Adv. Funct. Mater.* **33**, 2214405 (2023).
- 10 95. Y. He, Q. Li, L. Yang, C. Yang, D. Xu, Electrochemical-Conditioning-Free and Water-Resistant Hybrid $\text{AlCl}_3/\text{MgCl}_2/\text{Mg}(\text{TFSI})_2$ Electrolytes for Rechargeable Magnesium Batteries. *Angew. Chem. Int. Ed.* **131**, 7697-7701 (2019).
- 15 96. D. Aurbach *et al.*, Prototype systems for rechargeable magnesium batteries. *Nature* **407**, 724-727 (2000).
97. Z. Zhao *et al.*, Passivation Layers in Mg-Metal Batteries: Robust Interphases for Li-Metal Batteries. *Adv. Mater.* **36**, 2402626 (2024).
98. Y. Zhang, Y. Wu, H. Li, J. Chen, D. Lei, C. Wang, A dual-function liquid electrolyte additive for high-energy non-aqueous lithium metal batteries. *Nat. Commun.* **13**, 1297, (2022).
- 20 99. C. S. Rustomji *et al.*, Liquefied gas electrolytes for electrochemical energy storage devices. *Science* **356**, 1351 (2017).
100. Q. Zhao, S. Stalin, L. A. Archer, Stabilizing metal battery anodes through the design of solid electrolyte interphases. *Joule* **5**, 1119-1142 (2021).
- 25 101. Y. Li, *et al.*, Atomic structure of sensitive battery materials and interfaces revealed by cryo-electron microscopy. *Science* **308**, 506-510 (2017).
102. J. Zhang *et al.*, The origin of anode-electrolyte interfacial passivation in rechargeable Mg-metal batteries. *Energy Environ. Sci.* **16**, 1111-1124 (2023).
103. Y. Li, W. Huang, Y. Li, A. Pei, D. T. Boyle, Y. Cui, Correlating Structure and Function of Battery Interphases at Atomic Resolution Using Cryoelectron Microscopy. *Joule* **2**, 2167-2177 (2018).
- 30 104. C. Niu *et al.*, High-energy lithium metal pouch cells with limited anode swelling and long stable cycles. *Nat. Energy* **4**, 551-559 (2019).
105. G. Li *et al.*, Locking Active Li Metal through Localized Redistribution of Fluoride Enabling Stable Li-Metal Batteries. *Adv. Mater.* **33**, 2207310 (2023).
- 35 106. Y. Wang *et al.*, Electroless Formation of a Fluorinated Li/Na Hybrid Interphase for Robust Lithium Anodes. *J. Am. Chem. Soc.* **143**, 2829-2837 (2021).
107. X Ma *et al.*, Energy band-engineered solid electrolyte interphase for stable potassium-ion batteries. *Joule* **9**, 101952 (2025).
- 40 108. Q. Xu *et al.*, Li_2ZrF_6 -based electrolytes for durable lithium metal batteries. *Nature* **637**, 339 (2025).
109. O. Tamwattana *et al.*, High-dielectric polymer coating for uniform lithium deposition in anode-free lithium batteries. *ACS Energy Lett.* **6**, 4416-4425 (2021).
110. Y. Gao *et al.*, Polymer-inorganic solid-electrolyte interphase for stable lithium metal batteries under lean electrolyte conditions. *Nat. Mater.* **18**, 384-389 (2019).
- 45 111. C. Qin *et al.*, Tribo-electrochemistry induced artificial solid electrolyte interface by self-catalysis. *Nat. Commun.* **12**, 7184 (2021).
112. C. Fang *et al.*, Quantifying inactive lithium in lithium metal batteries. *Nature* **572**, 511-515

(2019).

113. G. M. Hobold, C. Wang, K. Steinberg, Y. Li, B. M. Gallant, High lithium oxide prevalence in the lithium solid-electrolyte interphase for high Coulombic efficiency. *Nat. Energy* **9**, 580-591 (2024).
- 5 114. S. Tan *et al.*, Unravelling the convoluted and dynamic interphasial mechanisms on Li metal anodes. *Nat. Nanotechnol.* **18**, 243-249 (2023).
115. C.-A. Lo *et al.*, Interdependence of Support Wettability-Electrodeposition Rate Sodium Metal Anode and SEI Microstructure. *Angew. Chem. Int. Ed.* **137**, e202412550 (2024).
116. S. B. Son *et al.*, An artificial interphase enables reversible magnesium chemistry in carbonate electrolytes. *Nat. Chem.* **10**, 532-539 (2018).
- 10 117. X. Huang, Asymmetric SO_3CF_3^- -Grafted Boron-Center Anion Enables Boron-Containing Interphase for High-Performance Rechargeable Mg Batteries. *Adv. Funct. Mater.* **34**, 2314146 (2024).
118. C. Bodin *et al.*, Boron-Based Functional Additives Enable Solid Electrolyte Interphase Engineering in Calcium Metal Battery. *Batteries & Supercaps* **6**, e202200433 (2022).
- 15 119. Q. Zhao *et al.*, Solid electrolyte interphases for high-energy aqueous aluminum electrochemical cells. *Sci. Adv.* **4**, eaau8131 (2018).
120. J. Forero-Saboya *et al.*, Understanding the nature of the passivation layer enabling reversible calcium plating. *Energy Environ. Sci.* **13**, 3423-3431 (2020).
- 20 121. J. Xiao *et al.*, Stable Solid Electrolyte Interphase In Situ Formed on Magnesium-Metal Anode by using a Perfluorinated Alkoxide-Based All-Magnesium Salt Electrolyte. *Adv. Mater.* **35**, 2203783 (2022).
122. S. Kumar, P. Rama, G. Yang, W. Y. Lieu, D. Chinnadurai, Z. W. Seh, Additive-Driven Interfacial Engineering of Aluminum Metal Anode for Ultralong Cycling Life. *Nano-Micro Lett.* **15**, 21 (2023).
- 25 123. D. A. Rakov *et al.*, Exploring the Impact of In Situ-Formed Solid-Electrolyte Interphase on the Cycling Performance of Aluminum Metal Anodes. *ACS Nano* **18**, 28456-28565 (2024).
124. J. Zhang *et al.*, Activation mechanism of conventional electrolytes with amine solvents: Species evolution and hydride-containing interphase formation. *J. Energy Chem.* **98**, 615-622 (2024).
- 30 125. X. Liang *et al.*, A facile surface chemistry route to a stabilized lithium metal anode. *Nat. Energy* **2**, 17119 (2017).
126. Z. Tu *et al.*, Fast ion transport at solid-solid interfaces in hybrid battery anodes. *Nat. Energy* **3**, 310-316 (2018).
- 35 127. D. Li *et al.*, Rational Design of an Artificial SEI: Alloy/Solid Electrolyte Hybrid Layer for a Highly Reversible Na and K Metal Anode. *ACS Nano* **16**, 16966-16975 (2022).
128. Y. Li *et al.*, Grain-Boundary-Rich Triphasic Artificial Hybrid Interphase Toward Practical Magnesium Metal Anodes. *Adv. Funct. Mater.* **33**, 2210639 (2023).
- 40 129. S. Kumar *et al.*, A Bi-based artificial interphase to achieve ultra-long cycling life of Al-metal anode in non-aqueous electrolyte. *Energy Storage Mater.* **65**, 103087 (2024).
130. F. Li *et al.*, A fluorinated alloy-type interfacial layer enabled by metal fluoride nanoparticle modification for stabilizing Li metal anodes. *Chem. Sci.* **10**, 9735-9739 (2019).
131. K. Tang *et al.*, A Stable Solid Electrolyte Interphase for Magnesium Metal Anode Evolved from a Bulky Anion Lithium Salt. *Adv. Mater.* **32**, 1904987 (2020).
- 45 132. Z. Chang, Y. Qiao, H. Deng, H. Yang, P. He, H. Zhou, A Liquid Electrolyte with De-Solvated Lithium Ions for Lithium-Metal Battery. *Joule* **4**, 1776-1789 (2020).
133. M. Wan *et al.*, Mechanical rolling formation of interpenetrated lithium metal/lithium tin

- alloy foil for ultrahigh-rate battery anode. *Nat. Commun.* **11**, 829 (2020).
134. A. Maddegalla *et al.*, AZ31 Magnesium Alloy Foils as Thin Anodes for Rechargeable Magnesium Batteries. *ChemSusChem* **14**, 4690-4696 (2021).
135. S. Huang *et al.*, Interfacial friction enabling ≤ 20 μm thin free-standing lithium strips for lithium metal batteries. *Nat. Commun.* **14**, 5678 (2023).
136. R. Raj *et al.*, Ternary Potassium-Bismuth-Telluride Intermetallic Support Promotes Electrochemical Stability in Potassium Metal Anodes. *Angew. Chem. Int. Ed.* **64**, e202502213 (2025).
137. G. Xu *et al.*, The Formation/Decomposition Equilibrium of LiH and its Contribution on Anode Failure in Practical Lithium Metal Batteries. *Angew. Chem. Int. Ed.* **60**, 7770-7776 (2021).
138. S. Fan, S. Cora, N. Sa, Evolution of the Dynamic Solid Electrolyte Interphase in Mg Electrolytes for Rechargeable Mg-Ion Batteries. *ACS Appl. Mater. Interfaces* **14**, 46635-46645 (2022).
139. H. Park *et al.*, Early Stage Li Plating by Liquid Phase and Cryogenic Transmission Electron Microscopy. *ACS Energy Lett.* **8**, 715-721 (2023).
140. C. Wang *et al.*, Trapping and imaging dynamic battery nanointerfaces via electrified cryo-EM. *Sci. Adv.* **11**, eadv3191 (2025).
141. S. C. Kim *et al.*, Data-driven electrolyte design for lithium metal anodes. *Proc. Natl. Acad. Sci. U.S.A.* **120**, e2214357120 (2023).
142. Y. Chen *et al.*, From Bulk to Interface: Solvent Exchange Dynamics and Their Role in Ion Transport and the Interfacial Model of Rechargeable Magnesium Batteries. *J. Am. Chem. Soc.* **146**, 12984-12999 (2024).
143. H. Wang *et al.*, Application-driven design of non-aqueous electrolyte solutions through quantification of interfacial reactions in lithium metal batteries. *Nat. Nanotechnol.* (2025).
144. T. Wang *et al.*, Fatigue of Li metal anode in solid-state batteries. *Science* **388**, 311-316 (2025).
145. W. Zhang *et al.*, Recovery of isolated lithium through discharged state calendar ageing. *Nature* **626**, 306-312 (2024).
146. S. Chen *et al.*, External Li supply reshapes Li deficiency and lifetime limit of batteries. *Nature* **638**, 676-683 (2025).
147. Y. Li *et al.*, Interfacial engineering to achieve an energy density of over 200 Wh kg⁻¹ in sodium batteries. *Nat. Energy* **7**, 511-519 (2022).
148. J. Chen *et al.*, Realizing an Energy-Dense Potassium Metal Battery at -40 °C via an Integrated Anode-Free and Dual-Ion Strategy. *J. Am. Chem. Soc.* **147**, 2393-2402 (2025).
149. Z. Huang *et al.*, A hundreds-milliampere-hour-scale solid-state aluminum-sulfur pouch cell. *Adv. Energy Mater.* **13**, 2302464 (2023).
150. J. A. Blázquez *et al.*, A practical perspective on the potential of rechargeable Mg batteries. *Energy Environ. Sci.* **16**, 1964-1981 (2023).

Acknowledgments:

Funding: J. L. was supported by the National Natural Science Foundation of China (No. 92372207 and 2023YFB2405802). Y. Y. was supported by Texas Center for Superconductivity at the University of Houston Core Funding Award. K. K. was supported by the National Research Foundation of Korea (NRF) grant funded by the Korea government (MSIT) (No. RS-2023-00261543) and Shell International Exploration & Production, Inc. Z. W. S. was supported by the

Singapore National Research Foundation (NRF Investigatorship NRF-NRFI09-0002) and the Agency for Science, Technology and Research (MTC Programmatic Fund M23L9b0052).

Competing interests: Y. L. is also affiliated with State Key Laboratory of Advanced Refractories, The Key Laboratory of High Temperature Electromagnetic Materials and Structure of MOE, Wuhan University of Science and Technology, Wuhan, 430081, People's Republic of China.

5

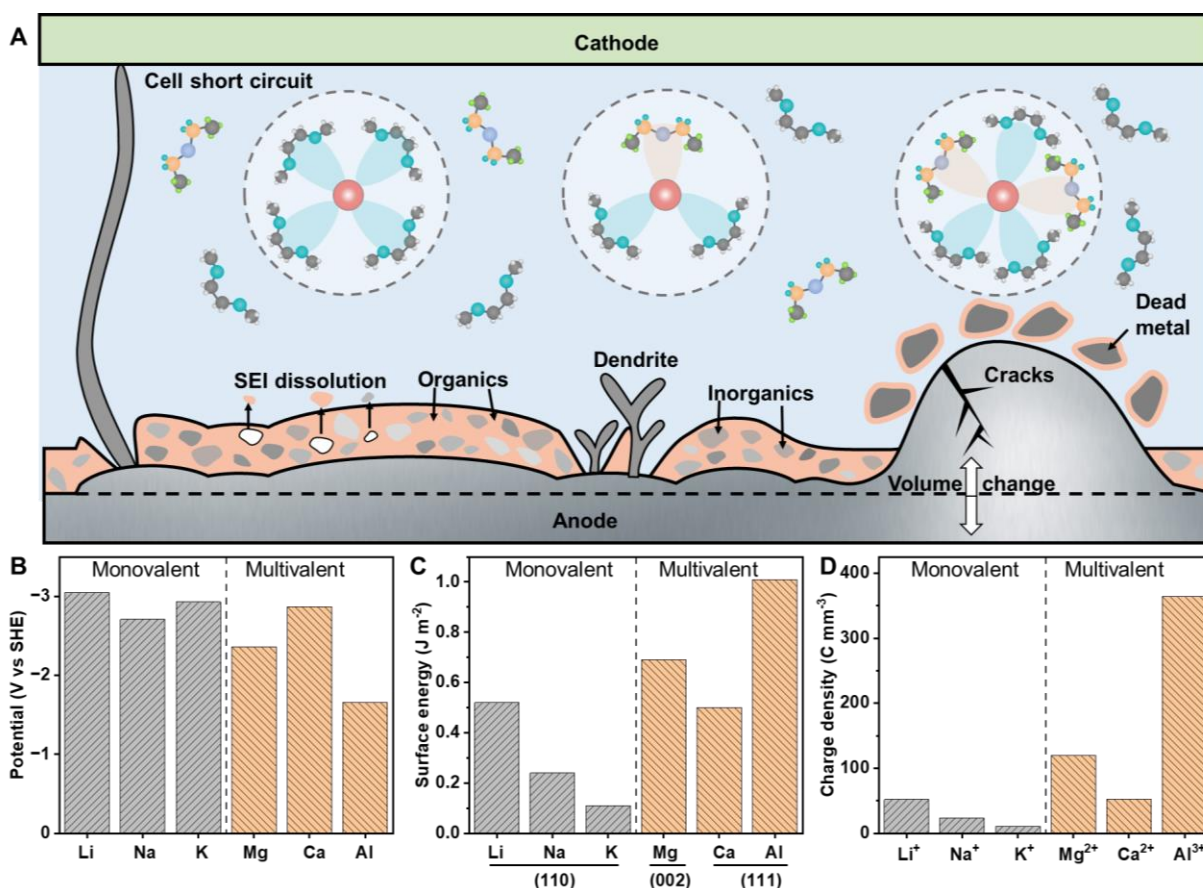


Fig. 1. Common challenges for monovalent and multivalent metal anodes. (A) Schematic showing the challenges for monovalent and multivalent metal anodes in conventional nonaqueous electrolytes, including uncontrolled growth of dendrite, spontaneous decomposition of electrolyte solvation structure, and subsequent formation of structurally inhomogeneous and compositionally unoptimized solid electrolyte interphase (SEI). During repeated plating and stripping, the organic and inorganic SEI components will dissolve in the electrolytes, and the huge volume change will cause SEI cracking and trigger the formation of electrochemically isolated “dead” metal. Meanwhile, the growth of metallic dendrites can proliferate in the interelectrode space to bridge the electrodes, giving rise to an early short-circuit cell failure in a working battery. These challenges are highly related to the intrinsic properties of monovalent and multivalent metal anodes and their coupled charge carriers, including (B) redox potential, (C) surface energy, and (D) charge density. Data obtained from (10, 20).

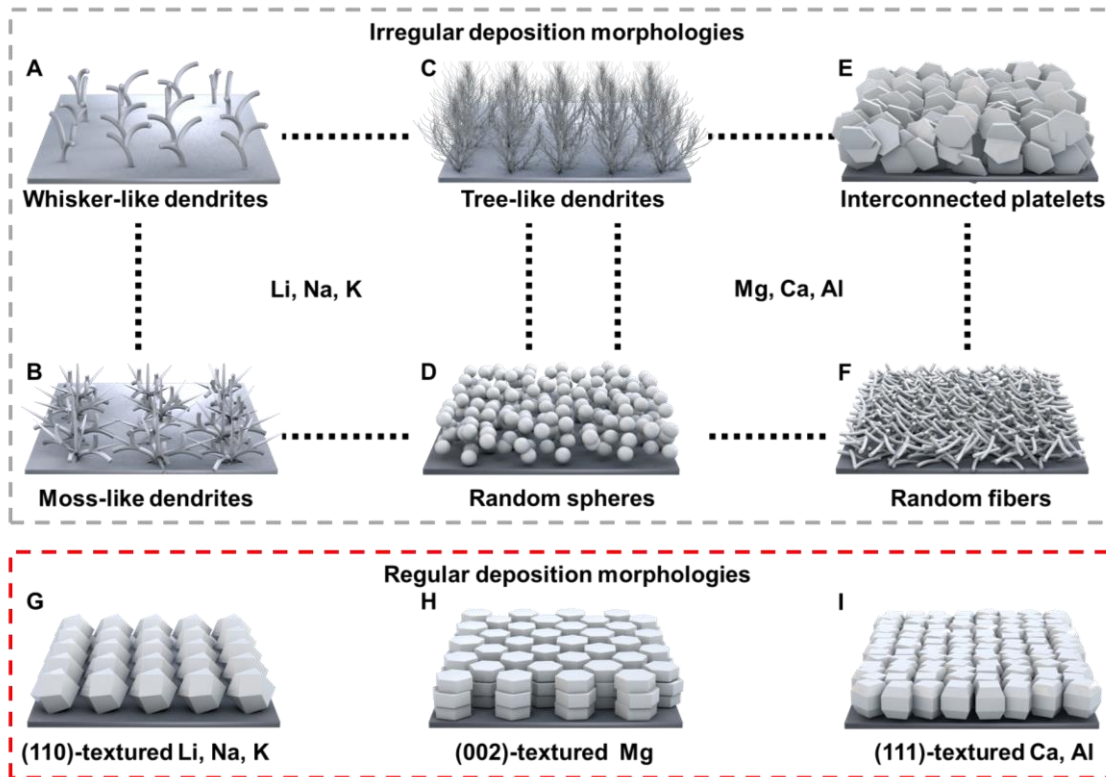


Fig. 2. Electroplating morphologies of monovalent and multivalent metals. Irregular deposition morphologies include (A) whisker-like dendrites, (B) moss-like dendrites, (C) tree-like dendrites, (D) random spheres, (E) interconnected platelets, and (F) random fibers, the first four of which are observed on monovalent metals while the last four of which are observed on multivalent metals. Regulated deposition morphologies include (G) (110) textured crystals for lithium, sodium, and potassium metals, (H) (002) textured crystals for magnesium metal, and (I) (111) textured crystals for calcium and aluminum metals.

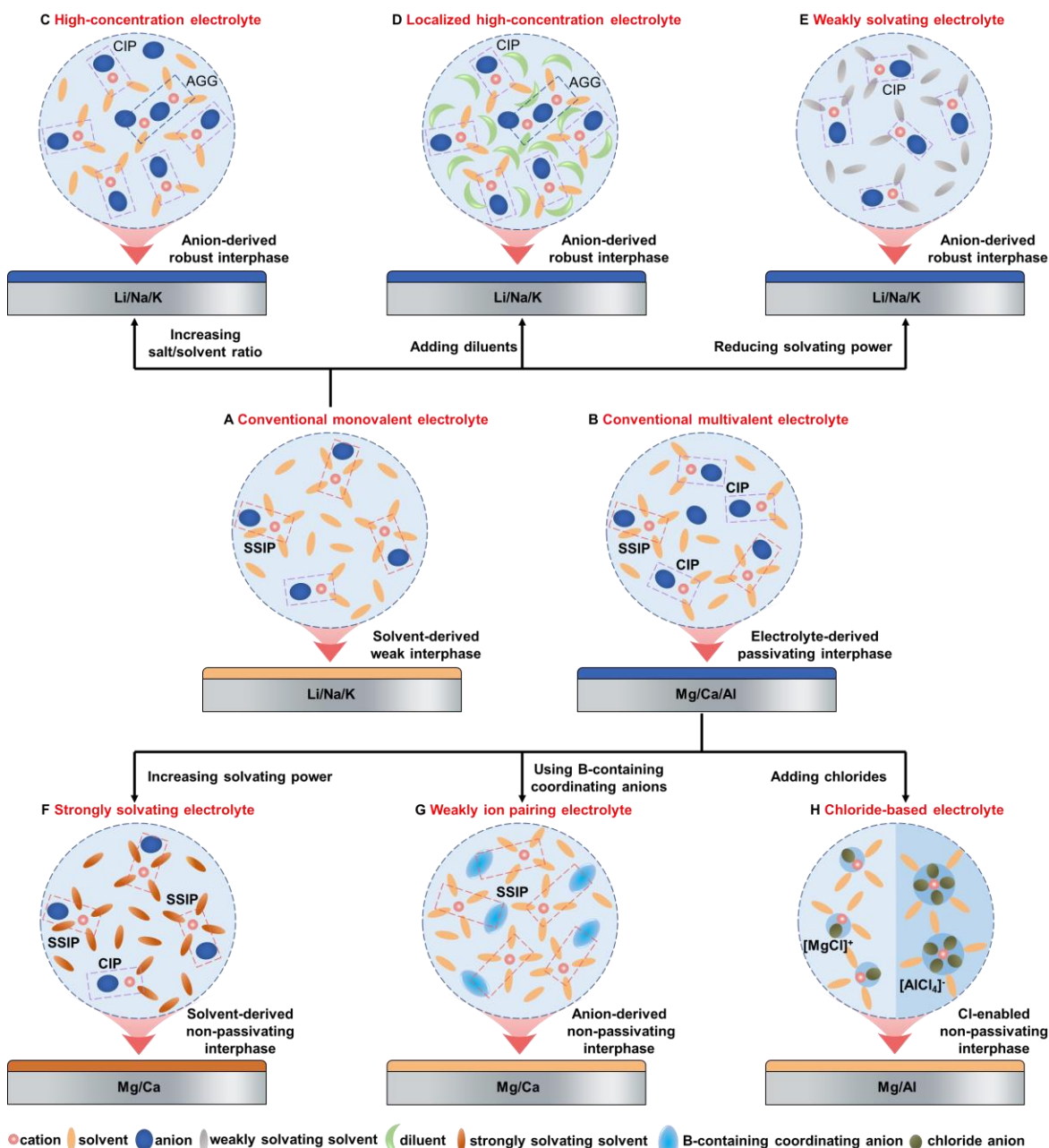


Fig. 3. Electrolyte solvation structure and associated interfacial chemistry for monovalent and multivalent metals. Schematic showing (A) conventional monovalent electrolytes with solvent-dominated solvation structures, which are easily reduced to form mechanically weak interphases on Li, Na, and K metals. Schematic showing the development of (C) weakly solvating electrolytes, (D) high-concentration electrolytes, and (E) localized high-concentration electrolytes to enable anion-participated solvation structure and anion-derived robust interphase for Li, Na, and K metals. Schematic showing (B) conventional divalent electrolytes with a large fraction of contact ion pairs, which aggravate passivation of Mg and Ca metals via pronounced electrolyte decomposition. Schematic showing the development of (F) strongly solvating electrolytes and (G) weakly ion-pairing electrolytes to enable regulated solvent-participated solvation structure and non-passivating interphase for Mg and Ca metals. (H) Schematic showing the existence of $MgCl^+$ or $AlCl_4^-$ complexes in chloride-based Mg or Al electrolytes, which can dissolve the passivation layer on Mg and Al metals.

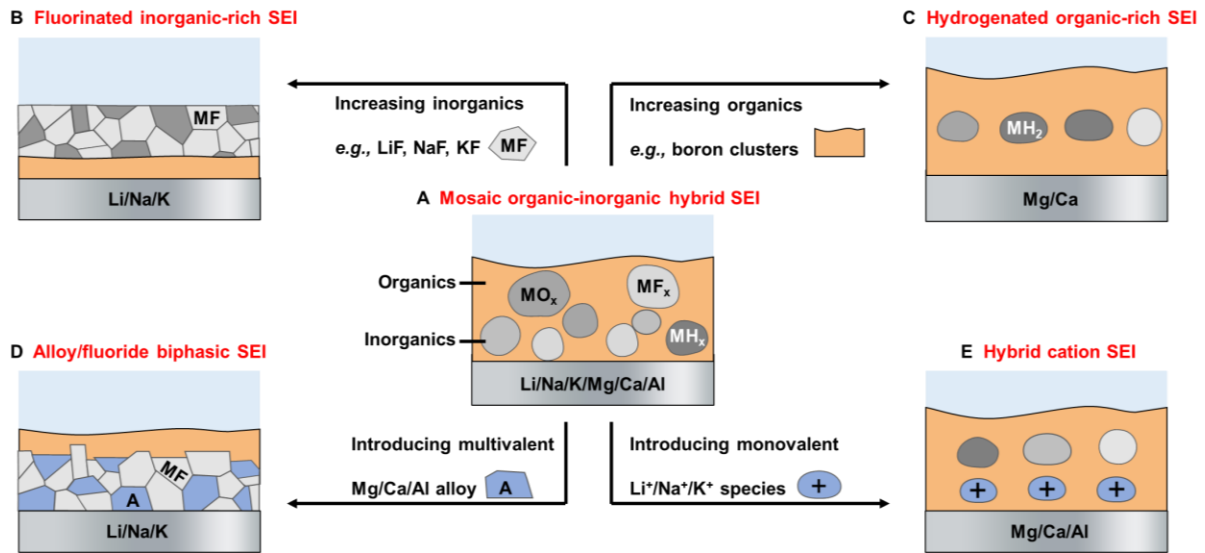
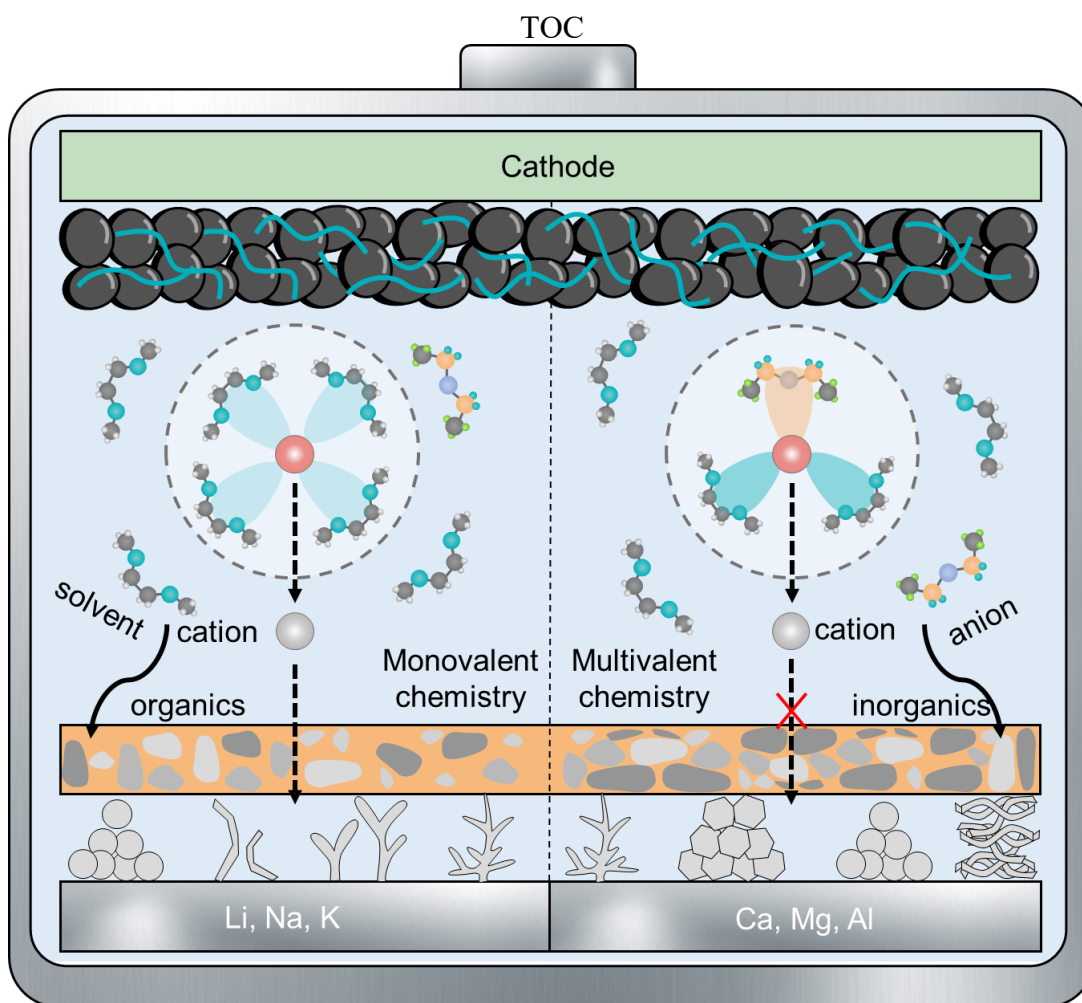


Fig. 4. Solid electrolyte interphase for monovalent and multivalent metals. Schematic showing (A) similar mosaic organic-inorganic hybrid SEI layers on Li, Na, K, Mg, Ca, and Al metal anodes. These structurally heterogeneous SEI layers trigger anisotropic ion transfer and uneven stress distribution, thereby leading to uncontrolled dendritic formation and early electrode failures. Schematic showing optimal (B) fluorinated inorganic-rich and (D) alloy/fluoride biphasic bilayer SEI layers for Li, Na, and K metal anodes, (C) hydrogenated organic-rich and (E) hybrid cation SEI layers for Mg, Ca, and Al metal anodes. These optimized SEI layers possess some universal merits of high ion conductivity, electronic insulation, (electro)chemical stability, and mechanically rigid-flexible synergy.



Electrochemical behavior of monovalent and multivalent metal anodes. In the monovalent battery (left), cations tend to coordinate with solvent molecules, forming a solvent-dominated electrolyte solvation structure that is easily reduced to form an organic-rich ion-conducting interphase. In the multivalent battery (right), the stronger Coulombic force of multivalent cations towards anions leads to an anion-participated electrolyte solvation structure, whose decomposition induces the formation of inorganic-rich ion-insulating interphases. Furthermore, unlike monovalent metals, which easily grow into whisker-like, moss-like, and tree-like dendrites, multivalent metals prefer deposition morphologies such as interconnected platelets and random fibers/spheres.

Summary

BACKGROUND: Batteries are an integral component of an electrified modern society, as they power consumer electronics/electric vehicles and help to integrate intermittent renewable energy into smart grids. With performance requirements constantly increasing, there is much demand for high-energy-density and low-cost batteries, beyond the capabilities of widely commercialized lithium (Li)-ion batteries. For a battery anode, Li metal is considered one of the most attractive choices because of its high theoretical specific capacity and negative electrochemical potential. Other promising anode candidates include sodium (Na), potassium (K), magnesium (Mg), calcium (Ca), and aluminum (Al) metals, as their crustal abundance is higher than that of lithium. Furthermore, all these monovalent (Li, Na, K) and multivalent (Mg, Ca, Al) metal anodes are indispensable for next-generation high-energy low-cost metal-sulfur and metal-air batteries.

ADVANCES: Following decades of research and development, the practical applications of these monovalent and multivalent metal anodes in nonaqueous rechargeable batteries are still plagued by common problems and specific challenges. (i) Irregular deposition is a common occurrence during electrochemical plating of Li, Na, K, Mg, Ca, and Al metals, however, the deposition morphologies are distinct for different metals. Specifically, monovalent metals easily grow into whisker-like, moss-like, and tree-like dendrites, whereas multivalent metals prefer deposition morphologies such as interconnected platelets and random fibers/spheres. There are also some reports of spherical dendrite growth for monovalent anodes and tree-like growth for multivalent anodes. (ii) Owing to their negative electrochemical potential, the considered metal anodes can readily react with electrolyte components such as solvents and salts to produce a heterogeneous interface layer, comprising both organics and inorganics. In monovalent batteries, Li^+ , Na^+ , and K^+ cations are mostly surrounded by solvent molecules (*e.g.*, 1,2-dimethoxyethane, DME), and the as-formed solvent-dominated solvation structure leads to the production of organic-rich solid-electrolyte interphases (SEI) on Li, Na, and K anodes, which permit the facile conduction of their respective ions. Differently, the multivalent nature of Mg^{2+} , Ca^{2+} , and Al^{3+} cations not only induces a strong tendency to form anion (*e.g.*, bis(trifluoromethanesulfonyl) imide, TFSI)-participated solvation structure in conventional nonaqueous electrolytes, but also tends to form inorganic-rich SEI layers. This makes it sluggish for multivalent cations with high charge density to diffuse across the nanointerface between the electrolyte and their corresponding metal anodes.

OUTLOOK: With a comprehensive understanding of the commonalities and differences in the electrochemical characteristics between monovalent and multivalent metal anodes, some general design principles and universal trends for these metal anodes emerge. (i) The desired deposition morphology for reversible metal cycling should comprise homogeneous and closely packed crystals with a specific crystallographic orientation, *e.g.*, (110) for Li, Na, and K, (002) for Mg, and (111) for Ca and Al. (ii) A favorable SEI usually requires similar homogeneous structures (*e.g.*, multilayer and monolithic structures) yet different chemical compositions (*e.g.*, fluorinated inorganic-rich SEI for Li, Na, and K, versus hydrogenated organic-rich SEI for Mg and Ca) to achieve some universal merits of high ion conductivity, electronic insulation, (electro)chemical stability, and mechanically rigid-flexible synergy. (iii) Smart electrolyte design strategies are required to achieve desired deposition morphology and SEI chemistries, *e.g.*, (locally) high salt concentration and weakly solvating electrolytes for monovalent systems, versus strongly solvating and weakly ion-pairing electrolytes for multivalent systems. The successful commercialization of these metal anode-based battery technologies further demands leveraging intrinsic advantages for specific applications, *e.g.*, high-energy Li metal batteries for long-range electric vehicles, cost-effective Na and K metal batteries for large-scale energy storage, and thermally resilient Mg, Ca, and Al metal batteries for extreme environment applications.